2006-11-10

M1 muscarinic receptors inhibit L-type Ca2+ current and M-current by divergent signal transduction cascades

Liwang Liu
University of Massachusetts Medical School

Et al.

Cellular/Molecular

M_1 Muscarinic Receptors Inhibit L-type Ca^{2+} Current and M-Current by Divergent Signal Transduction Cascades

Liwang Liu,[1,2] Rubing Zhao,[2] Yan Bai,[2] Lee F. Stanish,[2] James E. Evans,[3] Michael J. Sanderson,[2] Joseph V. Bonventre,[4] and Ann R. Rittenhouse[1,2]

[1]Program in Neuroscience and Departments of [2]Physiology and [3]Biochemistry and Molecular Pharmacology, University of Massachusetts Medical School, Worcester, Massachusetts 01655, and [4]Harvard Institute of Medicine, Harvard Medical School and Brigham and Women's Hospital, Boston, Massachusetts 02115

Ion channels reside in a sea of phospholipids. During normal fluctuations in membrane potential and periods of modulation, lipids that directly associate with channel proteins influence gating by incompletely understood mechanisms. In one model, M_1-muscarinic receptors (M_1Rs) may inhibit both Ca^{2+} (L- and N-) and K^+ (M-) currents by losing a putative interaction between channels and phosphatidylinositol-4,5-bisphosphate (PIP_2). However, we found previously that M_1R inhibition of N-current in superior cervical ganglion (SCG) neurons requires loss of PIP_2 and generation of a free fatty acid, probably arachidonic acid (AA) by phospholipase A_2 (PLA_2). It is not known whether PLA_2 activity and AA also participate in L- and M-current modulation in SCG neurons. To test whether PLA_2 plays a similar role in M_1R inhibition of L- and M-currents, we used several experimental approaches and found unanticipated divergent signaling. First, blocking resynthesis of PIP_2 minimized M-current recovery from inhibition, whereas L-current recovered normally. Second, L-current inhibition required group IVa PLA_2 [cytoplasmic PLA_2 ($cPLA_2$)], whereas M-current did not. Western blot and imaging studies confirmed acute activation of $cPLA_2$ by muscarinic stimulation. Third, in type IIa PLA_2 [secreted ($sPLA_2$)]$^{-/-}$/$cPLA_2^{-/-}$ double-knock-out SCG neurons, muscarinic inhibition of L-current decreased. In contrast, M-current inhibition remained unaffected but recovery was impaired. Our results indicate that L-current is inhibited by a pathway previously shown to control M-current over-recovery after washout of muscarinic agonist. Our findings support a model of M_1R-meditated channel modulation that broadens rather than restricts the roles of phospholipids and fatty acids in regulating ion channel activity.

Key words: **arachidonic acid; calcium current; M_1 muscarinic; phosphatidylinositol-4,5-bisphosphate; PIP_2; phospholipase A_2; plasticity; superior cervical ganglion; sympathetic**

Introduction

L-type Ca^{2+} (L-) channels are found throughout the nervous system, where they participate in many aspects of electrical activity, e.g., integrating synaptic input, encoding information in action potentials, and coordinating electrical activity at the cell membrane with underlying biochemical and transcriptional events (West et al., 2002; Marshall et al., 2003). Because L-channels are concentrated in cell bodies (Hell et al., 1993), their modulation by neurotransmitters may profoundly affect these processes. A well studied model of voltage-independent modulation is found in superior cervical ganglion (SCG) neurons, where M_1 muscarinic receptor (M_1R) agonists inhibit L-current (Suh and Hille, 2005). Although the changes in channel gating are understood (Mathie et al., 1992), the slow acting signal transduction pathway by which M_1Rs modulate L-channel activity remains uncharacterized.

This lack of information on L-current modulation contrasts the wealth of information known about M_1R inhibition of two other currents in SCG neurons, the K^+ current M-current and the N-type Ca^{2+} (N-) current. The first steps in the cascade involve M_1Rs coupling to G_q-like G-proteins (Haley et al., 2000) and phospholipase C (PLC) (Wu et al., 2002; Liu and Rittenhouse, 2003; Delmas and Brown, 2005; Suh and Hille 2005). Whether additional enzymes are required for M- and N-current modulation is controversial. Two models have been developed to explain the molecular events downstream of PLC leading to channel inhibition. The first model hypothesizes that loss of phosphatidylinositol-4,5-bisphosphate (PIP_2), normally associated with M- and N-channels, decreases channel activity (Suh and Hille, 2002; Wu et al., 2002; Ford et al., 2003; Zhang et al., 2003; Gamper et al., 2004). Our alternative model for N-current modulation proposes that inhibition requires generation of free fatty acid by phospholipase A_2 (PLA_2). This model is supported

Received Dec. 24, 2005; revised Sept. 7, 2006; accepted Sept. 14, 2006.

This work was supported by National Institutes of Health (NIH) Grants NS34195 (A.R.R.) and DK38452 (J.V.B.) and a Grant-In-Aid and an Established Investigator Award from the American Heart Association (A.R.R.). We acknowledge NIH Grant NS29632 to Glen Prestwich for the development of DBPC. Steve Farber, Glen Prestwich, and Taylor Rose provided advice in developing the imaging protocol. We thank Joshua J. Singer, Jim Hamilton, and Alan Kleinfeld for helpful discussions about fatty acid movement across membranes and their effects on ion channels and Trevor Shuttleworth for early advice on phospholipase inhibitors. We thank Eileen O'Leary for care of and genotyping the transgenic mice. We also thank Claire Baldwin, John F. Heneghan, Tora Mitra, Mandy L. Roberts, and John Walsh for critically reading various versions of this manuscript.

Correspondence should be addressed to Dr. Ann R. Rittenhouse, Program of Neuroscience, Department of Physiology, University of Massachusetts Medical School, 55 Lake Avenue North, Worcester, MA 01655. E-mail: ann.rittenhouse@umassmed.edu.

DOI:10.1523/JNEUROSCI.2102-06.2006

 0270-6474/06/2611588-11$15.00/0

by our findings that exogenously applied arachidonic acid (AA) mimicked muscarinic agonists and that antagonizing PLA_2 with oleyloxyethyl phosphorylcholine (OPC) or limiting free endogenous AA minimized whole-cell N-current modulation (Liu and Rittenhouse, 2003). However, OPC did not alter inhibition in perforated-patch recordings (Gamper et al., 2004), raising uncertainty about PLA_2 involvement. Moreover, whether L-current modulation requires PLA_2 remains untested. The conflicting interpretations of these findings underscore the importance of determining whether the same signaling cascade mediates inhibition of Ca^{2+} currents and M-current and whether the pathway entails simply a loss of PIP_2 (Suh and Hille, 2002) or requires additional phospholipid metabolism by PLA_2 (Liu and Rittenhouse, 2003).

To clarify these issues, the present study used pharmacological, biochemical, imaging, and genetic approaches to first investigate whether PLA_2 participates in L-current modulation. Here we report that L-current is inhibited by M_1Rs coupled to $G_{q/11}$, PLC/PIP_2, group IVa PLA_2 [cytoplasmic PLA_2 ($cPLA_2$)], and a free fatty acid, probably AA. We also tested whether M-current modulation requires PLA_2 and found that loss of PLA_2 activity dramatically slows M-current recovery from inhibition but exerts no effect on inhibition. Thus, L-current inhibition and M-current recovery use the same signaling cascade, whereas M-current inhibition requires only a decrease in PIP_2 levels. This unanticipated divergence in M_1R-mediated modulation of L- and M-current inhibition may contribute to neuronal plasticity.

Materials and Methods

Neonatal rat SCG neuron preparation. Dissociated sympathetic neurons were obtained from SCG of 1- to 4-d-old Sprague Dawley rats (Charles River Laboratories, Wilmington, MA) following the methods of Liu and colleagues (Liu et al., 2001; Liu and Rittenhouse, 2003). Cells were incubated at least 4 h before initiating whole-cell recording experiments and used within 12 h to avoid recording from cells with processes.

Adult SCG neuron preparation for electrophysiology and imaging. $cPLA_2^{-/-}$ mice were created by homologous recombination in J1 embryonic stem cells derived from 129/Sv mice and then introduced into C57BL/6J mice (Bonventre et al., 1997). The C57BL/6J × 129/Sv mice carry a spontaneous mutation that results in loss of secreted PLA_2 ($sPLA_2$). Thus, these mice are naturally $sPLA_2^{(-/-)}$, whereas the $cPLA_2^{-/-}$ mice are a PLA_2 double-knock-out and referred to as $s/cPLA_2^{(-/-)}$. Mice (8–16 weeks old) were decapitated, and their SCGs were removed and desheathed in Earle's balanced salt solution (EBSS) (Sigma, St. Louis, MO). Each ganglion was then cut into several pieces, transferred into a 25 cm^2 culture flask containing 5 ml of EBSS, 0.5 mg/ml trypsin (Worthington Biochemicals, Freehold, NJ), 1 mg/ml collagenase D (Roche Applied Science, Indianapolis, IN), 0.1 mg/ml DNaseI (Roche Applied Science), 3.6 g/L glucose, and 10 mM HEPES, and incubated at 34°C in a 5% CO_2/95% O_2 gassed, shaking water bath. After 1 h, the flask was shaken vigorously to release cell somata from ganglion fragments or dissociated by trituration with a P5000 Pipetman (Gilson, Middleton, WI). The dissociation was stopped by adding 5 ml of modified Eagle's medium (MEM) (Invitrogen, Carlsbad, CA) supplemented with 10% FBS, 4 mM glutamine, and 100 IU/ml penicillin–100 μg/ml streptomycin. Cells were pelleted by centrifuging at 500 × *g* for 5 min. For electrophysiological studies, the resulting pellet was resuspended in DMEM supplemented as for neonatal SCG neurons. Dissociated cells from the equivalent of one SCG were plated on poly-L-lysine-coated glass coverslips and incubated in Falcon (Franklin Lakes, NJ) 35 mm dishes at 37°C in a 5% CO_2 environment. SCG neurons were used within 12 h. For imaging studies, the pellet was gently resuspended in MEM, and a half ganglion was aliquoted into one 35 mm poly-L-lysine-coated glass-bottom Petri dish (number 1.5; MatTek, Ashland, MA) and incubated at 37°C in a 5% CO_2 environment.

Electrophysiological methods. Standard whole-cell recording methods and configuration were using following Liu and Rittenhouse (2003). Peak current amplitudes were measured 15 ms after the start of the test pulse. For experiments in which the long-lasting tail current was measured, a second cursor was placed ~13 ms after the test pulse.

The external solution for recording whole-cell Ca^{2+} currents contained the following (in mM): 135 *N*-methyl-D-glucamine-Asp, 10 HEPES, 20 Ba^{2+} acetate, and 0.0005 tetrodotoxin (TTX) (293 mOsm). The pipette solution contained the following (in mM): 123 Cs-Asp, 10 HEPES, 0.1 bis(2-aminophenoxy)ethane-*N*,*N*,*N*′,*N*′-tetra-acetic acid (BAPTA), 5 $MgCl_2$, 4 ATP, (Sigma), and 0.4 GTP (Sigma) (264 mOsm). The external solution used to record M-current contained the following (in mM): 160 NaCl, 2.5 KCl, 2 $CaCl_2$, 1 $MgCl_2$, 10 HEPES, and 8 glucose. The pipette solution contained the following (in mM): 175 KCl, 5 $MgCl_2$, 5 HEPES, 0.1 BATPA, 4 ATP, and 0.4 GTP.

As required for each experiment, drugs were added to the bath. Nimodipine (Miles, New Haven, CT), (+)-202-791 [S(+)-4-(2,1,3-benzoxadiazol-4-yl)-1,4-dihydro-2,6-dimethyl-5-nitro-3-pyridinecarboxylic acid isopropyl ester] (a gift from Sandoz, Basel, Switzerland), FPL 64176 (2,5-dimethyl-4-[2-(phenylmethyl)benzoyl]-1H-pyrrole-3-carboxylic acid methyl ester) (FPL) [Research Biomedicals (Natick, MA) or Sigma], 7,7-dimethyl-5,8-eicosadienoic acid (DEDA) (Sigma), OPC (Calbiochem, La Jolla, CA), and U-73122 (1-[6[[(17β)-3-methoxyestra-1,3,5(10)-trien-17-yl]amino]hexyl]-1H-pyrrole-2,5-dione) (Biomol, Plymouth Meeting, PA) were prepared as stock solutions in 100% ethanol and diluted with bath solution to a final ethanol concentration of <0.17% The maximal final concentration of ethanol had no significant effect on whole-cell peak or long-lasting tail currents. Stock solutions of AA (NuCheck, Elysian, MN) were kept under nitrogen at −80°C in sealed glass vials. Bovine serum albumin (BSA) (fraction V, heat shock, fatty acid ultra free; Roche Applied Science) was added directly to the bath solution. Stock solutions of oxotremorine-M (Oxo-M) (Tocris Cookson, Ellisville, MO), the G_q antagonist GPantagonist-2A (GPant2A) (Biomol), the mamba snake toxin MT-7 (Peptides International, Osaka, Japan), TTX (Sigma), and ω-conotoxin GVIA (ω-CgTX) (Bachem, Torrance, CA) made up in double distilled water were diluted at least 1000 times to their final concentration with bath solution. Oxo-M was used at a final concentration of 10 μM. Antagonists of the AA signaling cascade were used at concentrations shown previously to have just maximal inhibition in either the SCG or other cell systems. Supramaximal concentrations were avoided when possible to minimize cross-reactivity. IgG (1:1000 or 6.5 μg/ml; Calbiochem) or antibodies (Abs) selective for $G\alpha_{q/11}$ (1:1000 or 2.2 μg/ml; Calbiochem), $G\alpha_q$ (1:1000 or 2.2 μg/ml; Calbiochem), group IIa PLA_2 ($sPLA_2$; 1:250 or 0.8 μg/ml; Santa Cruz Biotechnology, Santa Cruz, CA), or group IVa PLA_2 ($cPLA_2$; 1:250 or 0.18 μg/ml; 1:500 or 0.09 μg/ml; Cell Signaling Technology, Beverly, MA) were included in the pipette solution.

Gas chromatography–mass spectrometric analysis of AA release from SCG. Adult rat SCGs were preincubated for 20 min at 37°C in 500 μl of EBSS in a shaking water bath gassed with 5% CO_2/95% O_2. 5,8,11,14-Eicosatetraynoic acid (30 μM; Sigma) was included in all EBSS solutions to block metabolism of AA. Ganglia were incubated for 10 min in the absence or presence of 0.5 mg/ml BSA. After stimulation, the incubation medium was immediately frozen in liquid nitrogen. Lipids were extracted from each sample by sequentially adding 1.5 ml of methanol, chloroform, and 0.88% KCl. The lower phase was removed, dried under nitrogen, and redissolved in 100 μl of chloroform/methanol (1:2). An aliquot (25 μl) was further processed for gas chromatography–mass spectrometric (GC–MS) analysis by converting the free fatty acids to their pentafluorobenzyl (PFBz) esters. That is, each sample had 100 ng of d3-phytanic acid added as an internal standard, was dried, redissolved in acetonitrile/triethylamine/pentafluorobenzyl bromide (50:10:5), and allowed to react at room temperature (22–24°C) for 15 min. Acetonitrile (200 μl) and *n*-hexane (1.0 ml) were added to each sample and mixed vigorously for 1 min. The hexane upper phase was removed, evaporated to dryness, and redissolved in 200 μl of *n*-hexane for analysis by negative ion electron capture chemical ionization (NCI) GC–MS analysis. GC–MS analyses were performed with a Waters Associates (Milford, MA) Quattro-II triple quadrupole mass spectrometry system equipped with an Agilent (Palo Alto, CA) 6890 gas chromatograph and Agilent

7683 autosampler. These analyses used a 30 × 0.25 mm inner diameter fused silica capillary column with a 0.25 μm DB-5 stationary phase coating (Agilent) and with helium as the carrier gas at 0.7 ml/min. Each sample (1 μl) was injected (injector, 300°C) in the splitless mode with the column at 185°C. After a 1 min hold at 185°C, the column temperature was programmed at 20°C/min to 240°C and then to 280°C at 5°C/min. Elution of the fatty acid PFBz esters was monitored by NCI GC–MS analysis with methane as the moderator gas at 4 e^{-4} mbar and the ion source at 150°C. Full scan spectra were acquired from m/z 223–345 with a cycle time of 0.5 s.

Reverse transcription-PCR analysis. RNA from 4-d-old SCG was isolated using Trizol (Invitrogen) according to the instructions of the manufacturer. Total RNA was resuspended in DEPC-treated water. Reverse transcription (RT) was performed using Omniscript RT kit (Qiagen, Alameda, CA) according to the instructions of the manufacturer. Group IVa PLA_2 transcripts were detected by PCR. A master mix contained 1.25 U of *Taq* polymerase, 1× Mg-free buffer, 1.5 mM $MgCl_2$, 200 mM dNTP mix (all from Promega, Madison, WI), and 0.24 μM forward and reverse primers (Invitrogen). Rat-specific primer sequences used were as follows: forward, 5′ ATG CTA ATG GCC TTG GTG AG 3′; and reverse, 5′ CTT GGC CTT GCA GAA AAG TC 3′. Mouse-specific primers used were as follows: forward, 5′ GGA AGC GAA CGA GAC ACT TC 3′; and reverse, 5′ CGA CTC ATA CAG TGC CTT CAT CAC 3′. RT at 10% was used as a DNA template per PCR reaction. After an initial denaturation step at 94°C for 5 min, samples were amplified using 40 cycles of 94°C for 30 s, 56°C for 45 s, and 72°C for 45 s. Samples were loaded onto agarose gels (1.8%); PCR products were separated by electrophoresis and visualized with ethidium bromide.

Oxo-M stimulation of adult SCG: Western blot analysis of phosphorylated $cPLA_2$. Pairs of adult ganglia were preincubated for 30 min at 37°C in EBSS gassed with 5% CO_2/95% O_2, as described previously (Rittenhouse and Zigmond, 1999). One ganglion was stimulated with 10 μM Oxo-M for 6 min. The contralateral ganglion served as an unstimulated control. After treatment, ganglia were homogenized on ice in lysis buffer containing 0.15 M NaCl, 5 mM EDTA, pH 8.0, 1% Triton X-100, 10 mM Tris-Cl, pH 7.4, and a protease inhibitor cocktail (Roche Diagnostics, Penzberg, Germany). The suspension was sonicated on ice for 15 s and incubated on ice for 30 min. Nuclear and cellular debris was removed by centrifugation at 14,000 × *g* for 10 min at 4°C. After determining protein content (RC/DC protein assay; Bio-Rad, Hercules, CA), lysates were loaded on either an 8 or 10% SDS-polyacrylamide gel. Proteins were separated by electrophoresis for 1 h and transferred to polyvinylidene difluoride membranes (Bio-Rad) using standard procedures.

Membranes were blocked overnight in PBS containing 5% (w/v) nonfat dry milk. Blots were probed for at least 1 h with Abs to either $cPLA_2$ (1:1000; Cell Signaling Technology) or to $cPLA_2$ phosphorylated at serine 505 (P-$cPLA_2$) (1:250; Cell Signaling Technology), washed, treated for 1 h with horseradish peroxidase (HRP)-conjugated secondary Abs (diluted 1:15,000; Bio-Rad), and rewashed. Membranes were developed using immuno-star HRP chemiluminescent kit (Bio-Rad) and exposed to film (Eastman Kodak, Rochester, NY). Membranes probed for $cPLA_2$ were stripped with 0.2N NaOH and reprobed with anti-β-actin Abs (1:10,000; Sigma). Membranes probed for P-$cPLA_2$ were reprobed with $cPLA_2$ Abs (1:250) as loading controls. After films were scanned with Fluor-S MultiImager (Bio-Rad), the density of the bands was analyzed with NIH ImageJ133 (http://rsb.info.nih.gov/ij/). Because equal numbers of ganglia were taken for control and stimulation, small differences in protein amount were corrected by normalizing the P-$cPLA_2$ signal to the $cPLA_2$ signal.

Immunocytochemistry of P-$cPLA_2$. Immunocytochemistry was performed to detect changes in P-$cPLA_2$ (Ser505) after stimulation with Oxo-M. Adult SCG neurons were cultured at low density at 37°C in MEM as above, for at least 16 h in a gridded chamber slide (Nagle Nunc, Rochester, NY) pretreated with poly-L-lysine. Under these conditions, little axonal outgrowth occurred, minimizing any potential synaptic or paracrine interactions among cells. Each chamber received a different experimental treatment. After stimulation, the chambers were removed, which allowed simultaneous processing of all cell groups for immunocytochemistry (22–24°C). Each slide was washed with PBS (two times for 5 min) and fixed with 100% acetone for 10 min, followed by three washes for 5 min with PBS. To identify principle neurons, cells were exposed to PBS containing 10% of normal goat serum for 60 min, followed by a 60 min exposure to 1:200 rabbit anti-tyrosine hydroxylase (TH) (Cell Signaling Technology) diluted in DakoCytomation (Carpinteria, CA) Antibody Diluent. Cells were washed with PBS (three times for 5 min) and incubated for 60 min in the dark with 1:200 Alexa Fluor 555 secondary anti-rabbit Ab (Invitrogen), diluted in DakoCytomation Antibody Diluent. After exposure to the secondary Ab, cells were again washed with PBS (three times for 5 min). The fixation and immunostaining protocols were repeated using 1:5000 rabbit anti-P-$cPLA_2$ (Cell Signaling Technology), followed by 1:200 Alexa Fluor 488 secondary anti-rabbit Ab. Slides were washed with distilled water and coated with the aqueous mounting medium Prolong Gold Antifade reagent (Invitrogen). Fluorescent images were visualized using a Nikon (Tokyo, Japan) Optiphot microscope and captured using Axio Vision 4.4 software (Zeiss, Oberkochen, Germany). Fluorescence intensity of each immunopositive cell was quantitated using NIH ImageJ133.

Confocal imaging of PLA_2 activity. Dissociated SCG neurons from $sPLA_2^{-/-}$ or $s/cPLA_2^{-/-}$ mice were loaded with 1-*O*-(6-Dabcyl-aminohexanoyl)-2-*O*-(6-[12-BODIPY-dodecanoyl]amino-hexanoyl)-*sn*-3-glycerylphosphatidylcholine (DBPC), a generous gift from Tyler Rose and Glenn Prestwich (Center for Cell Signaling, University of Utah and Echelon Biosciences, Salt Lake City, UT). A stock solution of DBPC (100 μg/100 μl chloroform) was prepared as described previously (B-7701 product information; Invitrogen), divided into 12 μl samples, dried with nitrogen, and stored at −80°C. Aliquots were redissolved in 12 μl of chloroform, mixed with 44 μl of phosphatidylserine (PS) (2 mg/ml chloroform; Avanti Polar Lipids, Alabaster, AL), and redried under nitrogen. DBPC–PS liposomes were kept in a desiccated environment (−20°C) in the dark. Liposomes were rehydrated with 1 ml of PBS, sonicated for 15 min on ice, and used within a few hours of preparation. Cells cultured in Matek dishes were preincubated in HBSS (Invitrogen) for 30 min. An aliquot (200 μl) of HBSS (total of 300 μl) was replaced with DBPC-labeled liposome and lightly mixed, yielding a final DBPC concentration of 0.01 μg/μl. Cells were incubated for 40 min at 37°C and washed three times with HBSS to remove any adherent liposomes. Cells were then viewed on a custom-built, video-rate confocal microscope (Sanderson and Parker, 2003) with a 40× objective lens. An excitation wavelength of 488 nm was used, and emission spectra were collected with long-pass filters at 515 nm (Perez and Sanderson, 2005). After recording time 0 images, cells were stimulated with Oxo-M or treated with HBSS for unstimulated control images. For each time point, images were collected at room temperature at 30 frames/s for 1 s using Video Savant (IO Industries, London, Ontario, Canada) and directly written to a personal computer. Each set of 30 images was averaged to create an image for time intervals ranging from 1 to 9 min and analyzed using NIH ImageJ133.

Statistical analysis. Data are expressed as the mean or percentage change ± SEM. Statistical significance was determined by either a two-way Student's *t* test for two means or a two-tailed paired *t* test. $p < 0.05$ was considered significant.

Results

M_1Rs, G_q, and PLC mediate slow pathway inhibition of M- and L-currents

To determine whether L-current inhibition by the slow pathway shares the same initial steps as those for M- and N-currents, M_1Rs, G_q, and PLC were blocked individually with selective antagonists (Fig. 1*A*). Cells were exposed to the muscarinic agonist Oxo-M plus each antagonist while L-current was monitored by two methods. First, preincubating cells with 1 μM ω-CgTX for at least 20 min minimized N-current. Under these conditions, the majority of the remaining current is L-current; thus, the ω-CgTX-insensitive current is referred to as L-current (for an additional explanation, see supplemental Fig. 1, available at www.jneurosci.org as supplemental material). Under these conditions, Oxo-M inhibited L-current 45 ± 6.6% ($n = 12$) (Fig. 1*B*,*C*). When MT-7, a selective mamba toxin antagonist of M_1Rs, was

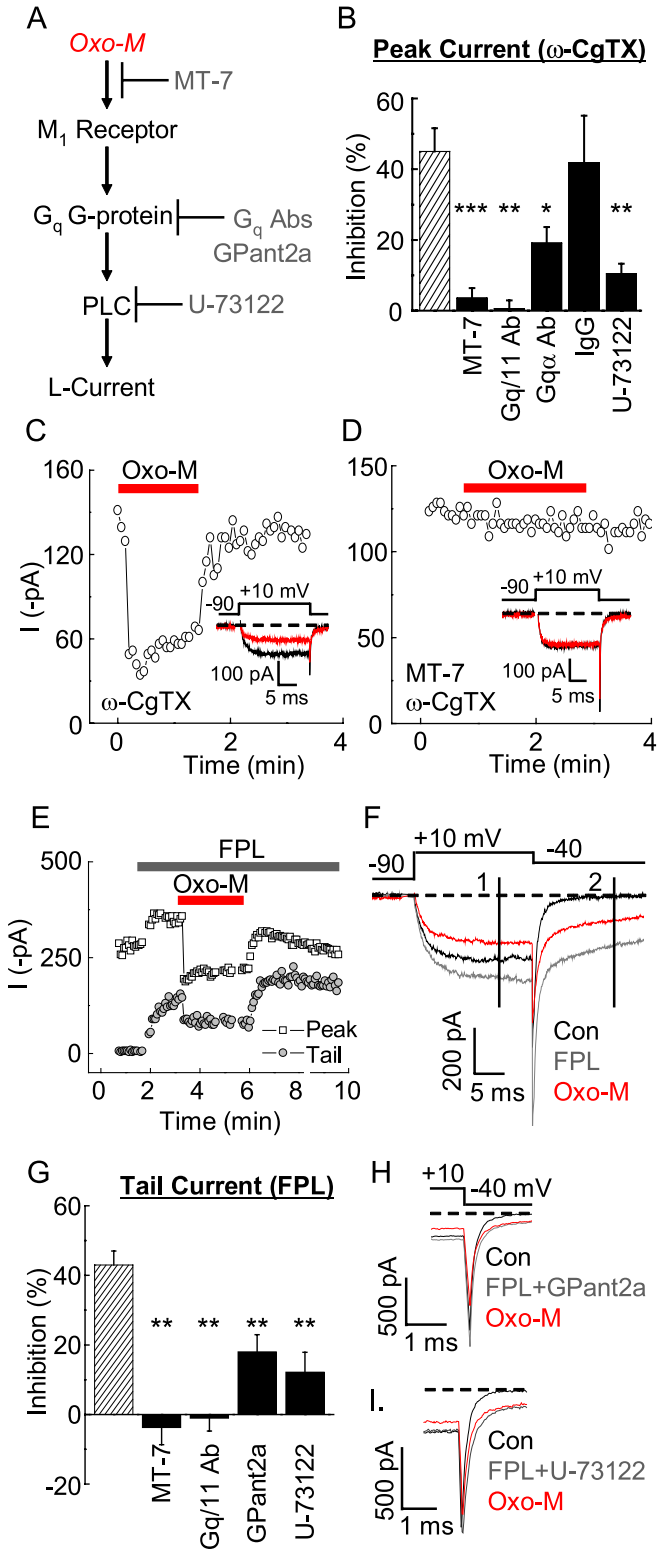

Figure 1. M_1Rs, G_q, and PLC mediate inhibition of L-current by the slow pathway. ***A***, Schematic illustrates the experimental strategy used to delineate the initial steps in the M_1R signal transduction cascade. In this and subsequent figures, currents were modulated with 10 μM Oxo-M. The M_1R-selective mamba snake toxin MT-7, the G_q antagonist GPant2A, G$\alpha_{q/11}$ and Gα_q Abs, and the PLC inhibitor U-73122 were tested for their ability to minimize current inhibition by Oxo-M. ***B–D***, N-channels were blocked by pretreating SCG neurons with 1 μM ω-CgTX for at least 30 min. ***B***, Summary of average percentage inhibition of L-current after Oxo-M treatment (hatched bar) or Oxo-M plus inhibitor (filled bars). $^*p < 0.05$, $^{**}p < 0.01$, $^{***}p < 0.001$ compared with no inhibitor, using a two-way *t* test for two means; $n = 4–11$ recordings per group. Example time course and selected sweeps (inset) illustrate current inhibition by Oxo-M under control conditions (***C***) and in the presence of 100 nM MT-7 (***D***). Fast tail currents of selected sweeps (***C***, ***D***) have been truncated. ***E–I***, L-current was isolated by a second method. Including the nondihydropyridine L-channel agonist FPL (1 μM) in the bath elicited a large, long-lasting tail current made up entirely of L-channel activity but only a modest increase of $20 \pm 5\%$ in peak current. ***E***, Oxo-M reversibly inhibited peak and long-lasting tail currents over time. ***F***, Locations of peak (1) and long-lasting tail (2) current measurements are shown in example sweeps taken from ***E***. ***G***, Summary of average percentage inhibition of the long-lasting tail current after Oxo-M treatment (hatched bar) or Oxo-M plus inhibitor (filled bars). $^{**}p <$ 0.01 compared with no antagonist using a two-way *t* test for two means; $n = 4–11$ recordings per group. ***H***, Examples of tail currents before FPL (Con), with FPL and GPant2A (10 μM), and ~1 min after Oxo-M in the continued presence of FPL and GPant2A (Oxo-M). ***I***, Inhibition of long-lasting tail currents was reduced in the presence of 2.5 μM U-73122. Con, Control.

included in the bath, Oxo-M no longer significantly inhibited the current (Fig. 1*B*,*D*). Second, including the L-channel agonist FPL in the bath elicited a long-lasting tail current comprising entirely L-current (Liu et al., 2001). Under these conditions, reversible muscarinic inhibition of the long-lasting tail current occurred but was also lost with MT-7 (Fig. 1*E–G*). These findings demonstrate that M_1Rs mediate muscarinic inhibition of L-current. When Abs selective for G$\alpha_{q/11}$ (Fig. 1*B*,*G*) or Gα_q (Fig. 1*B*) were included in the pipette solution as functional antagonists of G_q, L-current inhibition by Oxo-M decreased. In contrast, dialyzing neurons with non-immunized IgG (Fig. 1*B*) did not affect Oxo-M inhibition of L-current. GPant2A, a selective peptide antagonist of G_q G-proteins (Fig. 1*G*,*H*), and U-73122, a selective inhibitor of PLC (Fig. 1*B*,*G*,*I*), also antagonized Oxo-M-induced inhibition of L-current (for controls, see supplemental Fig. 2, available at www.jneurosci.org as supplemental material).

Wortmannin blocks recovery of M- but not L-current inhibition

The above data and previous work of others indicate that M_1Rs (Shapiro et al., 1999), G_q (Haley et al., 2000) and PLC, and therefore PIP_2 breakdown, are required for L-current modulation by the slow pathway similar to previous studies on whole-cell sympathetic Ca^{2+} currents (Wu et al., 2002), native N-current (Liu and Rittenhouse, 2003), and native and recombinant M-current (Suh and Hille, 2002). If the same signaling cascade modulates L- and M-currents, they should respond similarly to additional manipulations of the M_1R signaling cascade. When PIP_2 synthesis is blocked with a high concentration of wortmannin (10–50 μM), which antagonizes both phosphatidylinositol 3 kinase (IC_{50} of 5 nM) and phosphatidylinositol 4 (PI4) kinase (IC_{50} of 100 nM) (Nakanishi et al., 1995), M-current remains inhibited after washout of Oxo-M (Suh and Hille, 2002; Ford et al., 2003; Zhang et al., 2003). We also found that blocking PIP_2 synthesis with 10 μM wortmannin prevented recovery of M-current inhibition in adult SCG neurons (Fig. 2*A*,*B*,*D*). When we repeated this experiment with ω-CgTX-treated cells, wortmannin alone had no effect on L-current ($p > 0.10$ when comparing control currents with wortmannin; $n = 4$; data not shown). Oxo-M-induced L-current inhibition in the presence of wortmannin was normal. Moreover, inhibition of L-current reversed after ~1 min of washout (Fig. 2*C*,*D*).

L- but not M-current inhibition requires PLA_2 activity

The difference in L- and M-current sensitivities to wortmannin was unexpected. This difference may be attributable to L-current having a higher affinity for PIP_2. If so, a small amount of PIP_2 synthesis in the presence of wortmannin might account for full recovery. However, this mechanism seems unlikely because the

←

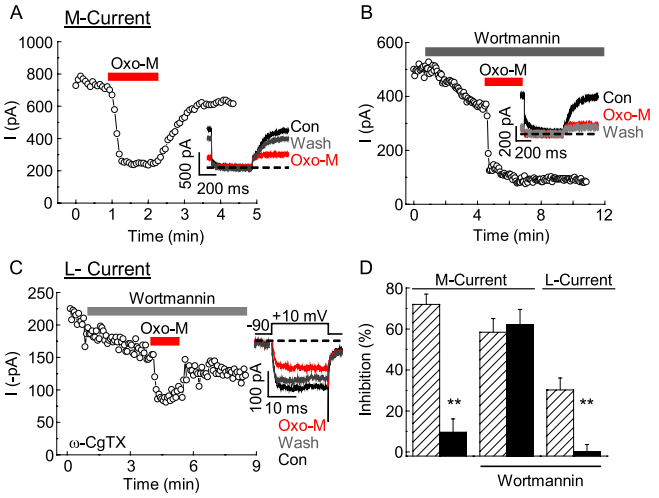

Figure 2. Wortmannin blocks recovery of M-current but not L-current. ***A***, Bath application of Oxo-M reversibly inhibits M-current in adult SCG neurons. Inset, Selected traces from the recording. ***B***, Wortmannin (10 μM) blocked M-current recovery from inhibition. Inset, Selected traces from the recording. ***C***, In contrast, L-current inhibition in neonatal SCG neurons reversed in the presence of wortmannin. Inset shows selected traces from the recording. The fast tail currents have been truncated. ***D***, Summary of L- and M-current inhibition by Oxo-M and their recovery in the presence of wortmannin. Under control conditions, Oxo-M inhibited M-current 72 ± 5% ($n = 6$). Inhibition (hatched bars) was readily reversible, with only 9.6 ± 6.5% inhibition remaining after ~1 min of washing (filled bars). In contrast, although the presence of wortmannin did not significantly change M-current inhibition by Oxo-M (58 ± 7%; $n = 4$), M-current remained inhibited by 62 ± 7.6% after 3 min of wash. Oxo-M-induced L-current inhibition in the presence of wortmannin was normal (30 ± 6%; $n = 6$) in ω-CgTX-treated cells ($p > 0.17$ when comparing percentage current inhibition of untreated to wortmannin-treated cells using a two-tailed t test for two means). Inhibition readily reversed, with 0.1 ± 3.6% remaining after ~1 min of washout. $^{**}p < 0.01$ compared with inhibition by Oxo-M using a two-tailed paired t test. Con, Control.

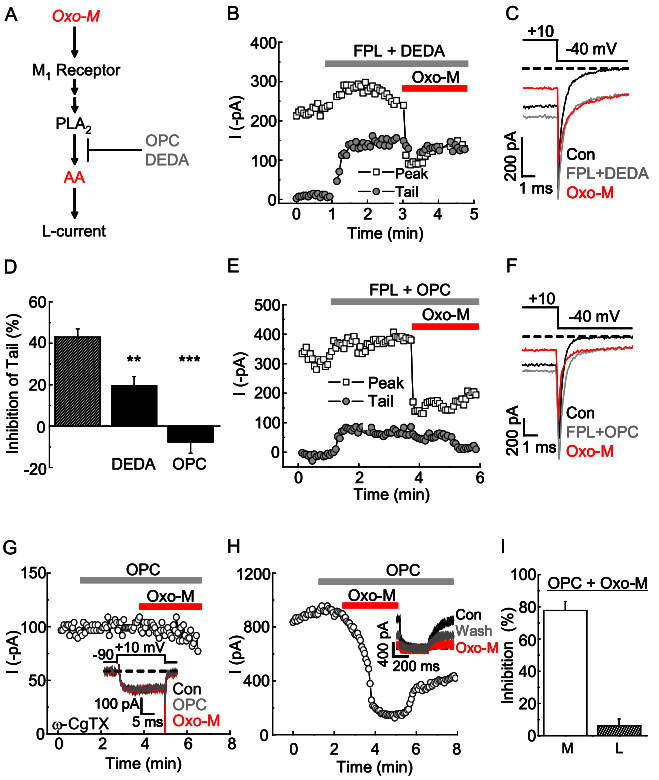

Figure 3. PLA_2 antagonists minimize L-current but not M-current inhibition by Oxo-M. ***A***, Schematic illustrating experimental protocol to test effects of selective PLA_2 antagonists, DEDA (IC_{50} of ~20 μM) and OPC (IC_{50} of 6 μM), on L-current modulation. ***B–F***, When FPL was included in the bath to enhance L-current, Oxo-M-induced inhibition of the long-lasting tail current was lost in the presence of either 100 μM DEDA (***B***, ***C***) or 10 μM OPC (***E***, ***F***). ***D***, Summary of the average percentage inhibition of the long-lasting tail current after Oxo-M treatment (hatched bar) or Oxo-M plus various PLA_2 inhibitors (filled bars): DEDA (100 μM; 20 ± 4%); OPC (10 μM; −8 ± 6%). $^{**}p < 0.01$, $^{***}p < 0.001$ compared with no inhibitor, using a two-way t test for two means; $n = 4–8$ recordings per group. ***G***, When cells were preincubated in ω-CgTX to block N-channel activity, Oxo-M-induced inhibition of L-current was minimized in the presence of OPC. Inset, Selected sweeps from the experiment; fast tail currents have been truncated. ***H***, Oxo-M inhibited M-current over time and in individual sweeps (inset) in the presence of OPC. ***I***, Summary of Oxo-M-induced inhibition of peak L-current ($n = 10$) in ω-CgTX-treated cells and of M-current ($n = 5$) in the presence of 10 μM OPC. Con, Control.

concentration of wortmannin used is 100 times greater than the IC_{50} for PI4 kinase. A second mechanism might explain our findings. Although L- and M-current inhibition by Oxo-M share initial steps in the signal transduction pathway, the pathways diverge after PIP_2 metabolism by PLC. This hypothesis is supported by our previous findings that N-current modulation by the slow pathway appears to require PLA_2 in addition to PLC (Liu and Rittenhouse, 2003).

To resolve whether inhibition of L- and/or M-current also requires PLA_2, we first used a pharmacological approach to examine PLA_2 participation in L-current inhibition. Four PLA_2 antagonists were tested for their ability to block L-current inhibition (Fig. 3*A*). Under the conditions used, none of them alone significantly altered control current levels (data not shown). First, 4-bromophenacyl bromide (BPB) was examined for its ability to block the inhibition of long-lasting tail currents by Oxo-M. In the presence of FPL and 20 μM BPB, Oxo-M inhibition of long-lasting tail current was essentially eliminated (data not shown). However the presence of BPB also significantly reduced muscarinic inhibition of the peak current to 14 ± 4% ($p < 0.05$; $n = 4$), suggesting that BPB may be disrupting not only the slow pathway but also the membrane-delimited pathway.

Therefore, we tested whether $AACOCF_3$ [arachidonyl trifluoromethylketone; Biomol], a second PLA_2 antagonist, could antagonize the actions of Oxo-M on ω-CgTX-treated neurons. When $AACOCF_3$ (50 μM) was dialyzed into cells for 5 min, Oxo-M inhibited the current by only 10 ± 5% ($n = 6$). Because these conditions did not allow us to manipulate the compound along with other bath-applied antagonists, we tested two additional antagonists (Fig. 3*B–D*). In the presence of DEDA (100 μM), inhibition of the long-lasting tail current by Oxo-M was significantly reduced to 19 ± 4% ($p < 0.01$; $n = 8$), whereas inhibition of the peak current remained (32 ± 5%; data not shown). In addition, DEDA decreased the inhibition of long-lasting tail current by Oxo-M when a different L-channel agonist, (+)-202–791 (1 μM), was used ($p < 0.05$; $n = 5$; data not shown), indicating that DEDA was not simply disrupting the actions of FPL.

Last, in the presence of OPC (10 μM), long-lasting tail current inhibition by Oxo-M was lost (Fig. 3*D–F*), whereas Oxo-M inhibited peak current by 39 ± 12% ($p < 0.02$ compared with unstimulated levels; $n = 4$). To verify the loss of L-current modulation in the presence of OPC, L-current was isolated by pretreating cells with ω-CgTX. When these cells were exposed to OPC, Oxo-M inhibited whole-cell current <10% (Fig. 3*G*,*I*). In contrast, OPC did not affect L-current inhibition by AA (Fig. 4*A–D*). These results indicate that OPC alone does not affect L-current and does not act nonselectively upstream of PLA_2 to disrupt either M_2R inhibition of N-current or general G-protein functioning nor act downstream of PLA_2 to block L-current in-

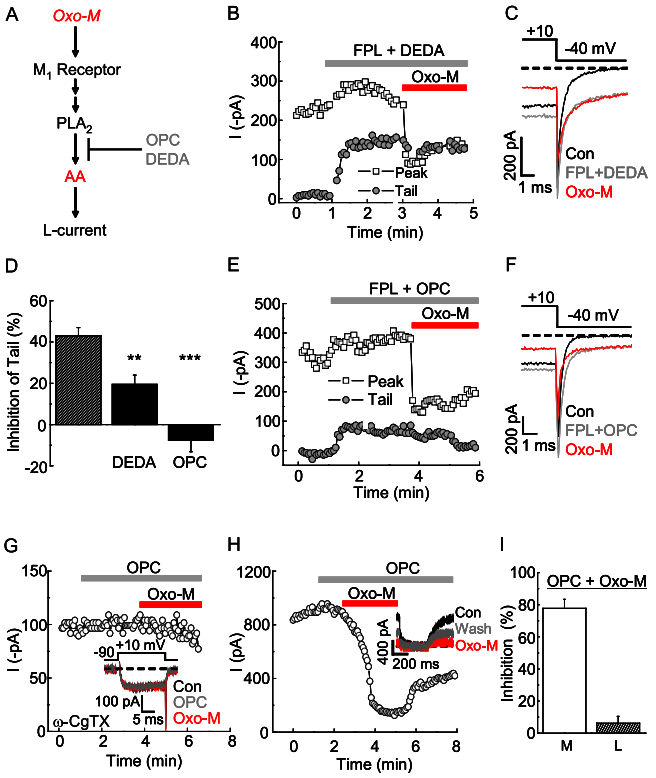

Figure 4. AA may participate in L-current inhibition by the slow pathway. ***A***, Schematic illustrates putative sites of action for OPC, BSA, and AA. ***B***, Example traces of AA-induced inhibition of long-lasting tail currents. ***C***, Example traces of AA-induced inhibition of long-lasting tail currents in the presence of 10 μM OPC. ***D***, Summary of the effects of 5–10 μM AA in the absence ($n = 6$) or presence ($n = 6$) of OPC. AA inhibited both the long-lasting tail current ($50 \pm 7\%$; $n = 6$) and peak current ($43 \pm 6\%$; $n = 6$), similar to its effects in the absence of OPC; $^*p < 0.05$ compared with control current levels when using a two-tailed paired *t* test. ***E***, Model by which BSA antagonizes M_1R modulation of channels. Control, After its liberation from phospholipids, AA diffuses from the inner to the outer lipid layer of the cell membrane. BSA, BSA binds free AA, facilitating its movement from the outer bilayer into the bath, consequently lowering AA levels in the bilayer and cytoplasm. AA binds to BSA well within several seconds, potentially fast enough to minimize any actions of AA liberated by M_1R stimulation (Kanterman et al., 1990). ***F***, The presence of BSA increased the amounts of AA found in the incubation medium of adult SCG stimulated with Oxo-M for 10 min. $^{***}p < 0.001$ compared with no BSA in the bath; $n = 5$ ganglia per group when using a two-way *t* test for two means. ***G***, In the presence of 1 μM FPL and 0.5 mg/ml BSA, Oxo-M rapidly and reversibly inhibited peak current, but inhibition of the long-lasting tail current was lost. ***H***, Selected sweeps from ***G***. ***I***, Summary of the effects of BSA ($n = 6$); $p > 0.05$ when comparing control (Con) with BSA group.

hibition by AA. Using a similar protocol, we found that Oxo-M in the presence of OPC inhibited M-current normally, but inhibition reversed by only $17 \pm 5\%$ ($n = 5$) after 2 min of wash compared with $62 \pm 6\%$ ($n = 6$; $p < 0.001$) in control recordings (Fig. 3*H*,*I*). These findings support a hypothesis in which L- and M-currents may be inhibited by divergent pathways.

Limiting endogenous AA minimizes L-current inhibition

Because L-current inhibition by Oxo-M requires PLA_2 and AA can inhibit L-current, we examined the relationship between Oxo-M and AA inhibition of L-current in three experiments. First, we documented that AA, like Oxo-M, inhibits FPL-induced long-lasting tail currents (Fig. 4*A*,*B*,*D*), as shown previously for peak L-current (Liu and Rittenhouse, 2000, 2003). Second, we found that the activation kinetics of L-currents were similar in the presence of either Oxo-M or AA and did not significantly change from those in FPL. For kinetic measurements, cells were preincubated with 1 μM ω-CgTX for at least 20 min to block N-current. In the continued presence of FPL (1 μM), cells were exposed to Oxo-M for 2 min. Oxo-M was washed out and 5 μM AA was introduced to the bath in the continued presence of FPL. The activation kinetics of L-current were measured for each condition from a composite of six traces. Current activation was best described by two time constants ($\tau_1 = 0.75 \pm 0.07$ ms; $\tau_2 = 8.31 \pm 0.90$ ms; $n = 9$). The fast and slow time constants did not significantly change in the presence of Oxo-M ($\tau_1 = 0.68 \pm 0.08$ ms; $\tau_2 = 7.98 \pm 1.06$ ms; $n = 8$) or AA ($\tau_1 = 0.54 \pm 0.10$ ms; $\tau_2 = 9.33 \pm 1.12$ ms; $n = 7$). Last, when Oxo-M was added after AA (10 μM), the long-lasting tail current was not inhibited further ($n = 3$; data not shown), indicating non-additivity of inhibition. The results from these three experiments are consistent with Oxo-M and AA using the same signal transduction pathway to inhibit L-current.

If release of endogenous AA mediates L-current modulation rather than decreased membrane levels of PIP_2, then exposing cells to BSA to lower the availability of AA should minimize L-current inhibition (Fig. 4*E*). Alternatively, if loss of PIP_2 is sufficient for L-current modulation as has been proposed for M-current (Suh and Hille, 2002), BSA should either leave inhibition intact or increase it by removing PIP_2 breakdown products. To test these possibilities, we included BSA in the bath and examined L-current inhibition by Oxo-M. Extracellular BSA rapidly binds AA (Spector, 1975), effectively scavenging free AA and other biologically active fatty acids that are present at the interface between the extracellular fluid and SCG nerve cell membranes (Fig. 4*E*). To demonstrate the effectiveness of this strategy, we incubated SCG with Oxo-M in the presence or absence of BSA and measured AA levels in the medium. AA levels were >10-fold higher in the presence of BSA than in its absence (Fig. 4*F*). Moreover, AA was undetectable (<0.1 ng) in BSA-containing medium that had not been exposed to an SCG (data not shown), demonstrating that the detected AA originated in the SCG. When BSA was included in the bath in whole-cell experiments, Oxo-M inhibition of the long-lasting tail current was lost (Fig. 4*G–I*). However, the peak current was significantly inhibited ($31 \pm 5\%$; $p < 0.001$; $n = 6$) because of the membrane-delimited pathway (Fig. 4*G*), indicating a selective loss of slow pathway modulation. These findings cannot explain a model in which L-channel activity decreases when PIP_2 dissociates from channels. Instead, our findings support a model in which AA is liberated from the membrane by Oxo-M stimulation of PLA_2. AA then acts either directly or indirectly to inhibit L-channel activity.

$cPLA_2$ is required for L-current inhibition by Oxo-M

We sought to identify the PLA_2 responsible for L-current modulation. PLA_2s generally fall into three categories: (1) secreted; (2) cytoplasmic and Ca^{2+} independent; or (3) cytoplasmic and Ca^{2+} dependent. Group IVa PLA_2 ($cPLA_2$), a cytoplasmic and Ca^{2+}-dependent PLA_2, was the likely phospholipase participating in the slow pathway for several reasons, most notably $cPLA_2$ preferentially hydrolyzes AA, versus other fatty acids found in the *sn*-2 position of phospholipids (Dennis, 1997). We detected $cPLA_2$ mRNA and protein in SCG using RT-PCR and Western blot analysis, respectively (Fig. 5*A*,*B*). Because phosphorylation of serine 505 by a number of kinases (e.g., protein kinase C and extracellular signal-regulated kinases 1 and 2) contributes to acute activation of $cPLA_2$ (Lin et al., 1992, 1993; Gijon et al., 1999), we tested whether muscarinic stimulation altered the levels of serine 505 phosphorylation as a measure of activation. When adult SCG were stimulated with Oxo-M for 6 min, Western blot analysis showed that $cPLA_2$ phosphorylation increased

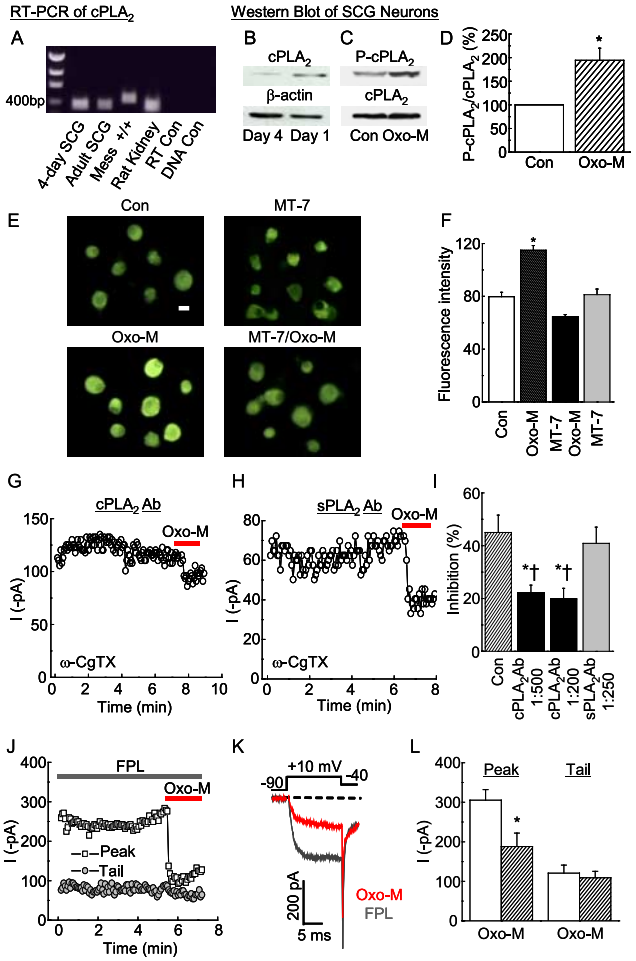

Figure 5. $cPLA_2$ antibody reduces L-current inhibition by Oxo-M. ***A***, RT-PCR amplification of $cPLA_2$ cDNAs. Total RNA isolated from different cells was used in RT-PCR reactions to amplify $cPLA_2$ cDNA. Rat-specific primers yielded a fragment of 340 bp for 4-d-old SCG, adult SCG, and rat kidney cells. Kidney cells were used as a rat-specific $cPLA_2$ positive control. Mouse-specific primers yielded a fragment of 476 bp for immortalized kidney mesangial cell line (Mess $^{+/+}$); these cells were used as a mouse-specific $cPLA_2$ positive control. RT Con (no homogenate) and DNA Con (no RT product) yielded no bands. ***B***, Western blot analysis of neonatal rat SCG homogenates demonstrates that the $cPLA_2$ Ab (1:1000) recognizes a single band at ~105 kDa. β-Actin Ab (1:10,000) served as a loading control. ***C***, Oxo-M significantly increased $cPLA_2$ phosphorylation at serine 505 (P-$cPLA_2$) in adult SCG. Ganglia were stimulated with Oxo-M for 5 min, with their contralateral SCG serving as unstimulated control. Blots were probed with Ab to P-$cPLA_2$, stripped, and reprobed with Ab to $cPLA_2$. ***D***, Summary of Western blot analysis ($n = 9$ blots). For each lane, P-$cPLA_2$ band density was normalized to that of the $cPLA_2$ band. $^*p < 0.05$, Oxo-M compared with unstimulated controls, using a two-way *t* test for two means. ***E***, Immunofluorescence of phosphorylated $cPLA_2$ in adult SCG neurons. Cells were preincubated in MEM in the absence (left column) or presence (right column) of MT-7 (100 nM) for 1 h at 37°C. Half of the cells served as unstimulated controls (top row), and the remaining cells were exposed to 10 μM Oxo-M (bottom row) for 10 min. Scale bar, 10 μm. After the stimulation, cells were immediately fixed and probed with primary Abs (for details, see Materials and Methods). Exposing cells only to secondary Ab yielded no $cPLA_2$-positive neurons (data not shown). ***F***, Summary of average immunofluorescence intensity (pixel units). Control, 80 ± 3.3 ($n = 42$ cells); Oxo-M, 115 ± 3.7 ($n = 58$ cells); MT-7 plus Oxo-M, 65 ± 1.7 ($n = 68$ cells); MT-7, 81 ± 4.3 ($n = 59$ cells). $^*p < 0.05$ compared with controls, MT-7 plus Oxo-M, or MT-7 groups. All cells analyzed were TH positive (data not shown). ***G***, Cells dialyzed with $cPLA_2$ Ab exhibit reduced L-current inhibition by Oxo-M over time. ***H***, In contrast, when cells were dialyzed with $sPLA_2$ Ab, Oxo-M inhibited the current. ***I***, Summary of the effects of PLA_2 Abs on Oxo-M-induced inhibition of L-current. $cPLA_2$ Ab at 1:200 to 20 ± 4%; $n = 8$. $^*p < 0.05$ compared with control, using a two-way *t* test for two means. $^\dagger p < 0.05$ compared with inhibition in cells dialyzed with $sPLA_2$ Ab (41 ± 6%; $n = 9$), using a two-way *t* test for two means. ***J***, Dialyzing $cPLA_2$ Ab into cells minimized long-lasting tail current inhibition by Oxo-M. Peak current still exhibited inhibition, most likely attributable to N-current modulation by the membrane-delimited pathway. ***K***, Consistent with membrane-delimited inhibition, inhibited currents exhibited slowed activation kinetics observed in individual sweeps taken from ***J***. ***L***, Summary of peak and long-lasting tail current inhibition by Oxo-M ($n = 6$). $^*p < 0.05$ compared with FPL level, using a two-tailed paired *t* test. Con, Control.

approximately twofold (Fig. 5*C*,*D*) with no change in the level of total $cPLA_2$.

Because the Western blot results demonstrated muscarinic stimulation of $cPLA_2$ phosphorylation, we tested whether stimulation of M_1Rs increased $cPLA_2$ phosphorylation in SCG neurons. Figure 5*E* documents that the Ab used in the Western blot analysis to detect phosphorylated $cPLA_2$ immunoreacted with dissociated adult SCG neurons, indicating the presence of $cPLA_2$ in dissociated rat SCG neurons. All neurons positive for TH were $cPLA_2$ positive (data not shown). SCG neurons, exposed to Oxo-M, displayed increased immunofluorescence (Fig. 5*F*). In contrast, exposing cells to Oxo-M in the presence of MT-7 blocked the increase in fluorescence, whereas MT-7 alone caused no change in fluorescence intensity. These findings demonstrate that M_1R stimulation accounts for the acute increase in $cPLA_2$ phosphorylation.

These findings indicated that Oxo-M acutely activates $cPLA_2$ in SCG. Therefore, we tested whether $cPLA_2$ is required for L-current modulation. Abs to $cPLA_2$ were dialyzed into ω-CgTX-treated SCG neurons via the patch pipette for 7–8 min. Oxo-M was then bath applied, and current inhibition was measured at +10 mV. Under these conditions, L-current inhibition by Oxo-M decreased significantly (Fig. 5*G*,*I*). In contrast, when cells were dialyzed with Abs to group IIa PLA_2 ($sPLA_2$), Oxo-M inhibited L-current normally (Fig. 5*H*,*I*). We confirmed a role for $cPLA_2$ by monitoring the long-lasting tail current in the presence of FPL (Fig. 5*J–L*). Under these conditions, the $cPLA_2$ Ab minimized inhibition of long-lasting tail current to <10%. In these same recordings, Oxo-M inhibited peak current by 40 ± 7% ($n = 6$), consistent with intact membrane-delimited inhibition of N-current.

Fatty acid release and L-current inhibition by Oxo-M are lost in SCG neurons lacking *cPLA$_2$*

If M_1R modulation of L-current requires $cPLA_2$, its absence should block the ability of Oxo-M to stimulate AA release from SCG neurons and subsequent L-current modulation. Taking a genetic approach, we used SCG neurons from C57BL/6J × 129/Sv mice lacking $cPLA_2$ to study Oxo-M-stimulated AA release and L-current inhibition. As with rat SCG neurons, wild-type mouse SCG neurons normally express $cPLA_2$ (Hornfelt et al., 1999). Interestingly, both the C57BL/6J and 129/Sv mouse strains have a naturally occurring background mutation in group IIa PLA_2 ($sPLA_2$) (Bonventre et al., 1997), a PLA_2 stimulated by effectors downstream from $cPLA_2$ (Murakami et al., 2000). Thus, C57BL/6J × 129/Sv $cPLA_2$ null mice are consequently double mutant animals ($sPLA_2^{-/-}/cPLA_2^{-/-}$) and are designated as $s/cPLA_2^{-/-}$. In contrast, littermate "control" mice are referred to as $sPLA_2^{-/-}$.

To determine whether SCG neurons from $s/cPLA_2^{-/-}$ adult mice exhibit decreased PLA_2 activity, we performed a fluorescence dequenching assay for PLA_2 using a fluorescently labeled phospholipid (Feng et al., 2002) detected with confocal imaging methods. In $sPLA_2^{-/-}$ SCG neurons exposed to Oxo-M, total cell fluorescence increased over time but decreased in unstimulated $sPLA_2^{-/-}$ neurons (Fig. 6*A*,*B*). In $s/cPLA_2^{-/-}$ SCG neurons, fluorescence decreased over time in both unstimulated and Oxo-M-treated neurons (Fig. 6*A*,*C*). The majority of the decrease is most likely attributable to photobleaching of the BODIPY moiety (see Materials and Methods). Figure 6*D* shows that Oxo-M-stimulated fluorescence rapidly increased over time in $sPLA_2^{-/-}$ neurons, and, at 6 min, fluorescence was 40% greater than that of $s/cPLA_2^{-/-}$ cells. These findings along with our $cPLA_2$ phosphor-

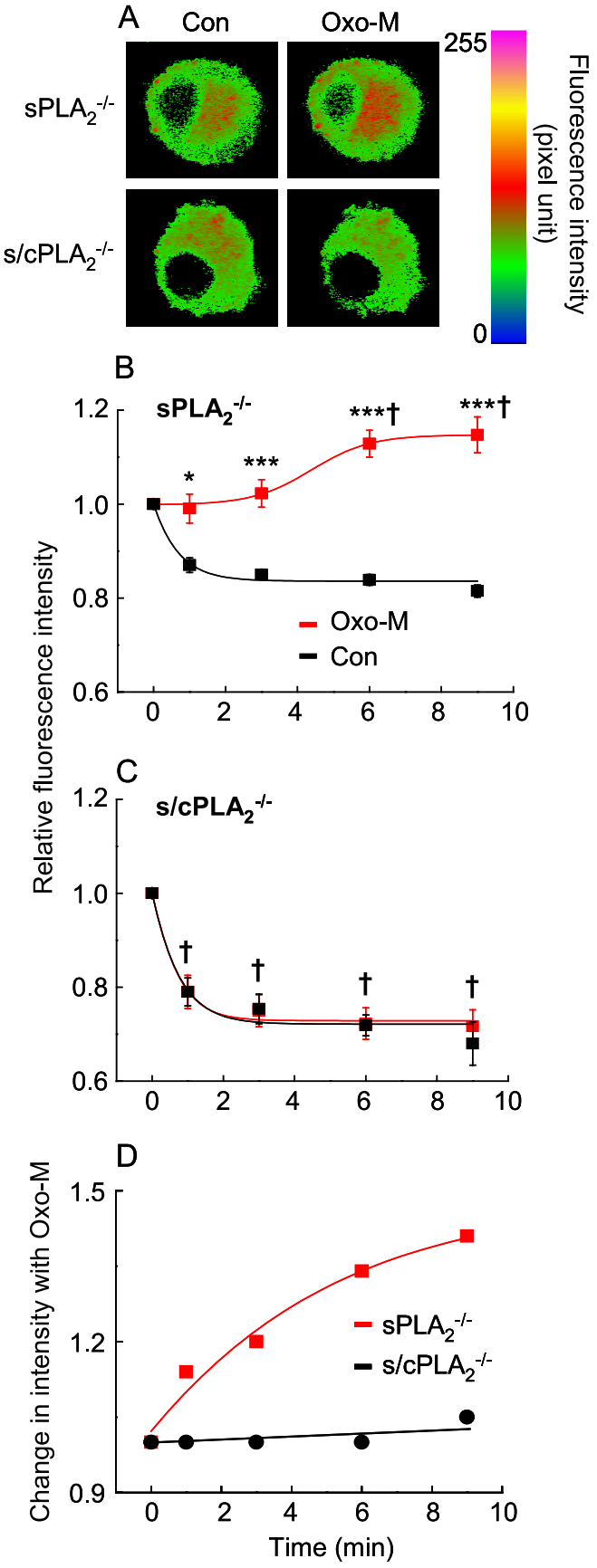

Figure 6. Oxo-M stimulates fatty acid release in $sPLA_2^{-/-}$ but not in $s/cPLA_2^{-/-}$ SCG neurons. PLA_2 activity was monitored using an engineered phosphatidylcholine molecule, DBPC. DBPC has a BODIPY-labeled fluorescent moiety attached to a fatty acid in the *sn*-2 position. A Dabcyl moiety, attached to the fatty acid in the *sn*-1 position, quenches the fluorescence of BODIPY. During cleavage, fluorescence of the BODIPY-labeled fatty acid is dequenched and detected as emission at 515 nm (Feng et al., 2002). Cells were preincubated for 40 min with DBPC to allow its uptake and equilibration among membrane compartments and washed to remove excess DBPC, and fluorescence was measured. ***A***, Examples of fatty acid fluorescence in $sPLA_2^{-/-}$ and in $s/cPLA_2^{-/-}$ mouse SCG neurons. Con, 0 min of stimulation; Oxo-M, 6 min exposure to Oxo-M. ***B***, ***C***, Time course of the changes in fluorescence for control or Oxo-M-stimulated $sPLA_2^{-/-}$ (***B***) and $s/cPLA_2^{-/-}$ (***C***) neurons. Fluorescence intensity was normalized to the 0 min time point. ***B***, $^{\dagger}p < 0.001$ (two-tailed paired *t* test) compared with 0 min of Oxo-M. $^{*}p < 0.05$, $^{***}p < 0.001$ compared with corresponding time point for control cells, using a two-way *t* test for two means. ***C***, $^{\dagger}p < 0.001$ for control and Oxo-M-treated neurons compared with 0 min using a two-tailed paired *t* test. Fatty acid fluorescence of control and Oxo-M-treated neurons did not differ at any time point. ***D***, Time course of fold change in fluorescence in stimulated compared with unstimulated neurons ($n = 10–20$ cells per group). Con, Control.

ylation and AA release studies show that Oxo-M-mediated activation of $cPLA_2$ increases free AA in SCG neurons within a time frame that could account for Oxo-M-induced decreases in L-current.

If AA, liberated by activated $cPLA_2$, participates in L-current modulation by the slow pathway, inhibition of L-current should be reduced in $s/cPLA_2^{-/-}$ SCG neurons. The slow pathway in mouse SCG neurons has similar characteristics to that in rat SCG neurons (Haley et al., 2000). However, mouse SCG neurons express not only L- and N-channels but also P/Q- and "R-"channels (Martinez-Pinna et al., 2002). Therefore, we examined modulation of L-current by testing whether inhibition of FPL-induced long-lasting tail currents was reduced in transgenic SCG neurons. Oxo-M inhibited the long-lasting tail current in $sPLA_2^{-/-}$ SCG neurons (Fig. 7*A*,*D*). In contrast, SCG neurons from conspecific $s/cPLA_2^{-/-}$ littermates exhibited no significant current inhibition by Oxo-M. However, Oxo-M significantly inhibited peak current, demonstrating selective loss of slow pathway modulation (Fig. 7*D*). The amplitudes of long-lasting tail currents did not differ in $s/cPLA_2^{-/-}$ and $sPLA_2^{-/-}$ neurons (Fig. 7*C*), indicating no inherent change in basal L-current between the two genetic backgrounds. Moreover, application of 5 μM AA inhibited current in ω-CgTX-treated $s/cPLA_2^{-/-}$ neurons (Fig. 7*D*), demonstrating that L-current sensitivity to AA remained intact. These findings indicate that L-current inhibition by the slow pathway requires $cPLA_2$.

In contrast, M-current inhibition was not significantly different between $sPLA_2^{-/-}$ and $s/cPLA_2^{-/-}$ SCG neurons (Fig. 8*A*,*B*). However, washout of inhibition was impaired in $s/cPLA_2^{-/-}$ neurons, similar to the OPC experiments (Fig. 3*H*). Inhibition in $s/cPLA_2^{-/-}$ SCG neurons recovered just 13 ± 8% ($n = 3$) compared with 46 ± 8% in $sPLA_2^{-/-}$ neurons ($n = 5$; $p < 0.05$) after 60 s of washing (Fig. 8*D*). To test whether the decreased rate of recovery observed in $s/cPLA_2^{-/-}$ neurons was attributable to a lack of liberated free fatty acid, we tested whether M-current in $sPLA_2^{-/-}$ neurons exhibited normal inhibition and washout when BSA was included in the bath. Under these conditions, Oxo-M inhibited current normally; however, M-current recovered from inhibition significantly less than in the absence of BSA, suggesting that generation of AA by $cPLA_2$ participates in M-current recovery from inhibition.

Discussion

This study compared the roles of PLA_2, AA, and PIP_2 in L- and M-current inhibition by muscarinic agonists. Inhibition of L-current by Oxo-M was minimized by blocking M_1Rs, G_q, or PLC with toxins, Abs, and/or selective antagonists. These findings are consistent with a model in which M_1R modulation of L-,

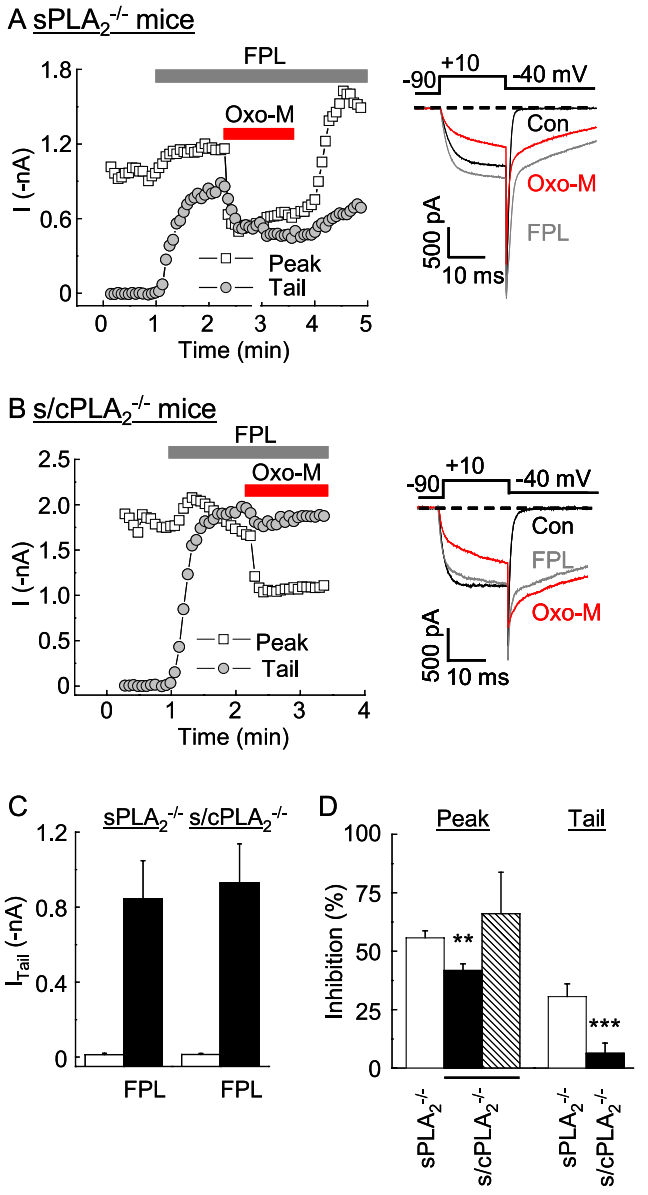

Figure 7. L-current inhibition by Oxo-M is reduced in $s/cPLA_2^{-/-}$ SCG neurons. ***A***, Oxo-M inhibited both peak (56 ± 3%) and long-lasting tail (31 ± 5%) currents ($n = 14$) in $sPLA_2^{-/-}$ SCG neurons. ***B***, In contrast, Oxo-M inhibited peak current by 42 ± 3% but long-lasting tail current by only 6 ± 4% ($n = 18$) in $s/cPLA_2^{-/-}$ neurons from conspecific littermates. Inhibition of peak current appears to be attributable to the membrane-delimited pathway, indicating that it remains active in transgenic neurons. ***C***, FPL enhanced long-lasting tail currents to a similar magnitude in $sPLA_2^{-/-}$ and $s/cPLA_2^{-/-}$ SCG neurons. ***D***, Summary of the effects of Oxo-M on peak and long-lasting tail currents in the presence of FPL. $^{**}p < 0.01$, $^{***}p < 0.001$, $s/cPLA_2^{-/-}$ (solid bars) compared with $sPLA_2^{-/-}$ (open bars) SCG neurons using a two-way *t* test for two means. Hatched bar, Peak current inhibition by 10 μM AA in ω-CgTX-treated neurons. Con, Control.

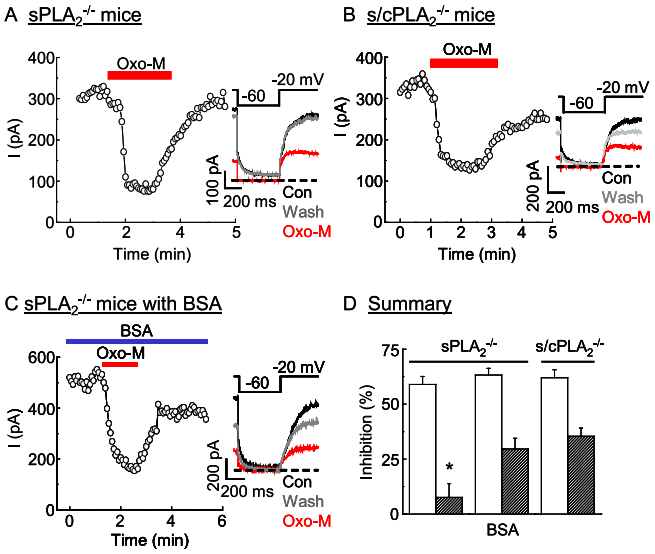

Figure 8. M-current inhibition by Oxo-M is normal in $s/cPLA_2^{-/-}$ SCG neurons. Bath application of Oxo-M inhibited M-current in $sPLA_2^{-/-}$ (***A***), $s/cPLA_2^{-/-}$ (***B***), and BSA-treated $sPLA_2^{-/-}$ (***C***) SCG neurons from C57BL/6J × 129/Sv mice. Insets, Selected traces taken from the recording. ***D***, M-current inhibition by Oxo-M was not significantly different ($p > 0.2$) among $sPLA_2^{-/-}$ (61 ± 6%; $n = 7$), $sPLA_2^{-/-}$ plus BSA (63 ± 3%; $n = 7$), and $s/cPLA_2^{-/-}$ (57 ± 4%; $n = 6$) neurons. M-current recovery was significantly greater in $sPLA_2^{-/-}$ SCG neurons ($^{*}p < 0.03$) than in BSA-treated $sPLA_2^{-/-}$ or in $s/cPLA_2^{-/-}$ SCG neurons. There was no significant difference in recovery among $s/cPLA_2^{-/-}$ and BSA-treated $sPLA_2^{-/-}$ SCG neurons ($p > 0.4$). Con, Control.

M-, and N-current involves the same second-messenger pathway (Shapiro et al., 2001; Suh and Hille, 2002, 2005; Wu et al., 2002). However, antagonizing PIP_2 synthesis with wortmannin, at a concentration that blocked recovery of M-current inhibition (Suh and Hille, 2002; Ford et al., 2003; Zhang et al., 2003), did not block recovery of L-current inhibition. These unexpected findings suggested that L-current was modulated differently from M-current.

We used biochemical, imaging, pharmacological, and genetic approaches to determine whether further phospholipid metabolism is required for L-current modulation. Our Western blot and immunocytochemical findings support a model in which Oxo-M acutely stimulates $cPLA_2$ phosphorylation, leading to acute enzyme activation and increased AA release from cell membranes. Consistent with phosphorylation acutely activating $cPLA_2$, our imaging studies show that Oxo-M stimulates fatty acid liberation in $cPLA_2$-containing ($sPLA_2^{-/-}$) but not in $s/cPLA_2^{-/-}$ neurons. Pharmacologically antagonizing PLA_2, dialyzing $cPLA_2$ Abs into cells, or using $s/cPLA_2^{-/-}$ neurons significantly decreased L-current inhibition by Oxo-M, indicating a requirement for $cPLA_2$. In particular, our finding that L-current inhibition by Oxo-M is lost in SCG neurons that do not express $cPLA_2$ is hard to interpret other than by concluding that $cPLA_2$ is required for modulation. The $s/cPLA_2^{-/-}$ mouse is well characterized (Bonventre et al., 1997). To date, $s/cPLA_2^{-/-}$ mice are known to differ biochemically from wild-type mice in one respect: they have decreased levels of cyclooxygenase-2 (COX-2) mRNA and protein (Bosetti and Weerasinghe, 2003). Decreased COX-2 in $s/cPLA_2^{-/-}$ SCG neurons is unlikely to account for the loss of L-current inhibition because we found no evidence that AA metabolism is required for L-current inhibition (Liu et al., 2001; Liu and Rittenhouse, 2003). Thus, we propose a pathway in which M_1R coupling to $G_{q/11}$ activates breakdown of PIP_2 by PLC. PLC and PLA_2 likely participate in the pathway sequentially because PLC activity also leads to protein kinase C and mitogen-activated protein kinase activation, followed by subsequent phosphorylation of $cPLA_2$ at Ser505 (Lin et al., 1992, 1993; Gijon et al., 1999). In turn, $cPLA_2$ liberates AA from membrane phospholipids, which directly or indirectly alters channel activity. Future studies are needed to determine the nature of the relationship between PLC and $cPLA_2$.

The possibility that PLA_2 participates in the slow pathway has been examined and rejected by other laboratories based on negative pharmacological findings. Gamper et al. (2004) reported that OPC did not affect the ability of Oxo-M to inhibit current recorded in the perforated-patch configuration from SCG neu-

rons. This result differed from our finding that OPC significantly decreased M_1R inhibition of N-current (Liu and Rittenhouse, 2003), a discrepancy that was attributed by Gamper et al. to differences in recording conditions. However, they did not report alternative experimental approaches or positive controls documenting active OPC. A second study examined the role of PLA_2 in L-current inhibition in HEK 293 cells transfected with M_1R rat $Ca_V1.2c$, $\alpha_2\delta$, and rabbit $\beta 2_a$ (Bannister et al., 2002). Muscarinic stimulation robustly inhibited whole-cell current. When PLC or PLA_2 activity was antagonized with U-73122 or quinacrine, respectively, M_1R-stimulated inhibition was unaffected (Bannister et al., 2002). Interestingly, we previously found that quinacrine as high as 1 mM did not inhibit purified $cPLA_2$, whereas 100 μM DEDA, the concentration used in our patch-clamp experiments, antagonized $cPLA_2$ activity by 80% (Kim and Bonventre, 1993). No positive controls were presented in the $Ca_v1.2c$ study; thus, it is unclear whether conditions were suboptimal for the antagonists. A more interesting possibility is that M_1Rs could modulate $Ca_V1.2c$ differently than wild-type L-current in SCG neurons, which is thought to arise from $Ca_V1.3$ (Lin et al., 1996). At present, however, we know of no sequence variability that might explain these differences. Nevertheless, these studies raise interesting questions as to whether all types of L-channels, including splice variants (Safa et al., 2001; Liao et al., 2004), express the same critical residues to mediate channel inhibition by the slow pathway.

Our model involving AA participation in slow pathway inhibition of L-current is supported by a growing list of findings. (1) AA mimics inhibition of L-channel activity by Oxo-M recorded in whole-cell and cell-attached patch configurations (Mathie et al., 1992; Liu and Rittenhouse, 2000, 2003; Liu et al., 2001). (2) The kinetics of Oxo-M-inhibited L-currents are statistically indistinguishable from those in the presence of AA. (3) AA occludes L-current inhibition by Oxo-M. (4) Decreasing the availability of free AA by including BSA in the bath antagonized L-current inhibition by Oxo-M. If loss of PIP_2 decreased channel activity, BSA should not have affected or should have increased the magnitude of current inhibition because BSA binds fatty acids and effectively removes them from solution, promoting further metabolism of PIP_2. It is hard to reconcile the decrease in Oxo-M-induced L-current inhibition in the presence of BSA with a model proposing that current is inhibited when PIP_2 dissociates from channels.

How AA inhibits L-current is unknown, but several theories have been proposed. AA may mediate M_1R signaling by activating additional downstream molecules such as kinases (Gailly et al., 1997; Liao et al., 2004) or phosphatases, as has been proposed for AA-mediated inhibition of T- and cardiac L-currents (Petit-Jacques and Hartzell, 1996; Zhang et al., 2000) and AA-mediated M-current enhancement (Yu, 1995). This model does not require a loss of PIP_2 bound to channels. In a second scenario, AA could occupy a critical position around the channel, competing with PIP_2 for the same site of interaction (Liu et al., 2004), as has been proposed for some K^+ channels (Rogalski and Chavkin, 2001). A third possibility is that AA acts directly on the channel at a site distinct from PIP_2. This model has been proposed for K_v currents in which PIP_2 binding to A-type K_v channels eliminates N-type fast inactivation. In contrast to the actions of PIP_2, AA promotes a rapid form of inactivation, converting non-inactivating, delayed rectifier K_v currents into fast-inactivating, A-type K_v currents (Oliver et al., 2004). These findings document a critical, stabilizing, structural role for both AA and PIP_2 interactions with K^+ channels at distinct sites. Our analysis of unitary L-channel activity found that AA increased the percentage of null sweeps, consistent with stabilizing either a closed or inactivated state (Liu and Rittenhouse, 2000). At the whole-cell level, AA increased holding potential-dependent inactivation (Liu et al., 2001), suggesting an increase in C-inactivation. The opposing actions of PIP_2 (Wu et al., 2002; Gamper et al., 2004) and AA on Ca^{2+} currents (Liu and Rittenhouse, 2000; Liu et al., 2001; Zhang et al., 2003; Talavera et al., 2004) appear remarkably similar to those for K_v currents, suggesting that their actions may be conserved across a number of voltage-gated ion channel families, including Ca^{2+} channels.

These conserved actions of PIP_2 and AA may extend to M-current in which M-channel availability to open increases with PIP_2 (Zhang et al., 2003). However, M-current is not inhibited by AA nor does PLA_2 activity participate in M-current inhibition by M_1Rs, as demonstrated previously in NG108 cells (Robbins et al., 1993) and here in SCG neurons. We examined whether OPC or BSA antagonized M-current inhibition by Oxo-M. Neither agent changed inhibition compared with control conditions. These findings were confirmed in transgenic studies; Oxo-M inhibited M-current similarly in $sPLA_2^{-/-}$ and $s/cPLA_2^{-/-}$ SCG neurons. We interpreted these differences as indicators that a diverging M_1R signaling cascade differentially inhibits L- and N-current from M-current. Moreover, our unanticipated findings that OPC, BSA, or the absence of $cPLA_2$ greatly attenuated M-current recovery from inhibition indicated a role for $cPLA_2$ and AA in recovery from the inhibitory process. A role for AA in regulating M-current is supported by the finding that exogenously applied AA enhances M-current in frog sympathetic neurons (Villarroel, 1994; Yu, 1995).

Together, these results indicate that M-current inhibition requires only PIP_2 breakdown, whereas L- and N-current inhibition and M-current recovery also require generation of a fatty acid, probably AA, by $cPLA_2$. These differences indicate that AA uses additional, novel mechanisms to regulate M-current compared with Ca^{2+} channels and other K_v channel activity (Oliver et al., 2004). Moreover, this signaling cascade appears remarkably similar to the PLA_2-sensitive pathway responsible for M-current over-recovery observed after washing out of agonist in other cell types (Robbins et al., 1993; Villarroel, 1994; Yu, 1995). Mechanistically, these unexpected findings suggest that, to observe the effects of AA on recovery, sufficient PIP_2 must be present in the membrane and/or associated with the channels. Our model of M_1R-meditated channel modulation thus broadens rather than restricts the roles of phospholipids and fatty acids in regulating ion channel activity. At the cellular level, the consequence of channel modulation by M_1R stimulation is to depolarize membranes and increase action potential firing in sympathetic (Brown and Adams, 1980) and cortical (Hamilton et al., 1997; Potier and Psarropoulou, 2004) neurons. These findings indicate that the slow pathway acts within a neural network to regulate the particular excitability state of a neuron. Such a process is thought to be involved in the release of modulatory transmitters from cortical projections to regulate attention and working memory (Goldman-Rakic, 1999; Mechawar et al., 2000).

References

Bannister RA, Melliti K, Adams BA (2002) Reconstituted slow muscarinic inhibition of neuronal ($Ca_v1.2c$) L-type Ca^{2+} channels. Biophys J 83:3256–3267.

Bonventre JV, Huang Z, Taheri MR, O'Leary E, Li E, Moskowitz MA, Sapirstein A (1997) Reduced fertility and postischaemic brain injury in mice deficient in cytosolic phospholipase A_2. Nature 390:622–625.

Bosetti F, Weerasinghe GR (2003) The expression of brain cyclooxygenase-2 is down-regulated in the cytosolic phospholipase A_2 knockout mouse. J Neurochem 87:1471–1477.

Brown DA, Adams PR (1980) Muscarinic suppression of a novel voltage-sensitive K^+ current in a vertebrate neuron. Nature 283:673–676.

Delmas P, Brown DA (2005) Pathways modulating neural KCNQ/M (Kv7) potassium channels. Nat Rev Neurosci 6:850–862.

Dennis EA (1997) The growing phospholipase A_2 superfamily of signal transduction enzymes. Trends Biochem Sci 22:1–2.

Feng L, Manabe K, Shope JC, Widmer S, DeWald DB, Prestwich GD (2002) A real-time fluorogenic phospholipase A_2 assay for biochemical and cellular activity measurements. Chem Biol 9:795–803.

Ford CP, Stemkowski PL, Light PE, Smith PA (2003) Experiments to test the role of phosphatidylinositol 4,5-bisphosphate in neurotransmitter-induced M-channel closure in bullfrog sympathetic neurons. J Neurosci 23:4931–4941.

Gailly P, Gong MC, Somlyo AV, Somlyo AP (1997) Possible role of atypical protein kinase C activated by arachidonic acidic in Ca^{2+} sensitization of rabbit smooth muscle. J Physiol (Lond) 500:95–109.

Gamper N, Reznikov V, Yamada Y, Yang J, Shapiro MS (2004) Phosphotidylinositol 4,5-bisphosphate signals underlie receptor-specific Gq/11-mediated modulation of N-type Ca^{2+} channels. J Neurosci 24:10980–10992.

Gijon MA, Spencer DM, Kaiser AL, Leslie CC (1999) The role of phosphorylation sites and the C2 domain in regulation of cytosolic phospholipase A_2. J Cell Biol 145:1219–1232.

Goldman-Rakic PS (1999) The physiological approach: functional architecture of working memory and disordered cognition in schizophrenia. Biol Psychiatry 46:650–661.

Haley JE, Delmas P, Offermanns S, Abogadie FC, Simon MI, Buckley NJ, Brown DA (2000) Muscarinic inhibition of calcium current and M current in Gαq-deficient mice. J Neurosci 20:3973–3979.

Hamilton SE, Loose MD, Qi M, Levey AI, Hille B, McKnight GS, Idzerda RL, Nathanson NM (1997) Disruption of the M_1 receptor gene ablates muscarinic receptor-dependent M current regulation and seizure activity in mice. Proc Natl Acad Sci USA 94:13311–13316.

Hell JW, Westenbroek RE, Warner C, Ahlijanian MK, Prystay W, Gilbert MM, Snutch TP, Catterall WA (1993) Identification and differential subcellular localization of the neuronal class C and class D L-type calcium channel α_1 subunits. J Cell Biol 123:949–962.

Hornfelt M, Edström A, Ekström PAR (1999) Upregulation of cytosolic phospholipase A2 correlates with apoptosis in mouse superior cervical and dorsal root ganglia neurons. Neurosci Lett 265:87–90.

Kanterman RY, Ma AL, Briley EM, Axelrod J, Felder CC (1990) Muscarinic receptors mediate the release of arachidonic acid from spinal cord and hippocampal neurons in primary culture. Neurosci Lett 118:235–237.

Kim DK, Bonventre JV (1993) Purification of a 100 kDa phospholipase A_2 from spleen, lung and kidney: antiserum raised to pig spleen phospholipase A_2 recognizes a similar form in bovine lung, kidney and platelets, and immunoprecipitates phospholipase A_2 activity. Biochem J 294:261–270.

Liao P, Yu D, Lu S, Tang Z, Liang MC, Zeng S, Lin W, Soong TW (2004) Smooth muscle-selective alternatively spliced exon generates functional variation in Cav1.2 calcium channels. J Biol Chem 279:50329–50335.

Lin LL, Lin AY, Knopf JL (1992) Cytosolic phospholipase A2 is coupled to hormonally regulated release of arachidonic acid. Proc Natl Acad Sci USA 89:6147–6151.

Lin LL, Wartmann M, Lin AY, Knopf JL, Seth A, Davis RJ (1993) cPLA2 is phosphorylated and activated by MAP kinase. Cell 72:269–278.

Lin Z, Harris C, Lipscombe D (1996) The molecular identity of Ca channel alpha 1-subunits expressed in rat sympathetic neurons. J Mol Neurosci 7:257–267.

Liu L, Rittenhouse AR (2000) Effects of arachidonic acid on unitary calcium currents in sympathetic neurons. J Physiol (Lond) 525:391–404.

Liu L, Rittenhouse AR (2003) Arachidonic acid mediates muscarinic inhibition and enhancement of N-type Ca^{2+} current in sympathetic neurons. Proc Natl Acad Sci USA 100:295–300.

Liu L, Barrett CF, Rittenhouse AR (2001) Arachidonic acid both inhibits and enhances whole cell calcium currents in rat sympathetic neurons. Am J Physiol Cell Physiol 280:C1293–C1305.

Liu L, Roberts ML, Rittenhouse AR (2004) Phospholipid metabolism is required for M_1 muscarinic inhibition of N-type calcium current in sympathetic neurons. Eur Biophys J 33:255–264.

Marshall J, Dolan BM, Garcia EP, Sathe S, Tang X, Mao Z, Blair LA (2003) Calcium channel and NMDA receptor activities differentially regulate nuclear C/EBPbeta levels to control neuronal survival. Neuron 39:625–639.

Martinez-Pinna J, Lamas JA, Gallego R (2002) Calcium current components in intact and dissociated adult mouse sympathetic neurons. Brain Res 951:227–236.

Mathie A, Bernheim L, Hille B (1992) Inhibition of N- and L-type calcium channels by muscarinic receptor activation in rat sympathetic neurons. Neuron 8:907–914.

Mechawar N, Cozzari C, Descarries L (2000) Cholinergic innervation in adult rat cerebral cortex: a quantitative immunocytochemical description. Comp Neurol 428:305–318.

Murakami M, Nakatani Y, Kuwata H, Kudo I (2000) Cellular components that functionally interact with signaling phospholipase A(2)s. Biochim Biophys Acta 1488:159–166.

Nakanishi S, Catt KJ, Balla T (1995) A wortmannin-sensitive phsophatidylinositol 4-kinase that regulates hormone-sensitive pools of inositol phospholipids. Proc Natl Acad Sci USA 92:5317–5321.

Oliver D, Lien C-C, Soom M, Baukrowitz T, Jonas P, Fakler B (2004) Functional conversion between A-type and delayed rectifier K^+ channels by membrane lipids. Science 304:265–270.

Perez JF, Sanderson MJ (2005) The frequency of calcium oscillations induced by 5-HT, ACH and KCl determine the contraction of smooth muscle cells of intrapulmonary bronchioles. J Gen Physiol 125:535–553.

Petit-Jacques J, Hartzell HC (1996) Effect of arachidonic acid on the L-type calcium current in frog cardiac myocytes. J Physiol (Lond) 493:67–81.

Potier S, Psarropoulou C (2004) Modulation of muscarinic facilitation of epileptiform discharges in immature rat neocortex. Brain Res 997:194–206.

Rittenhouse AR, Zigmond RE (1999) Role of N- and L-type calcium channels in depolarization-induced activation of tyrosine hydroxylase and release of norepinephrine by sympathetic cell bodies and nerve terminals. J Neurobiol 40:137–148.

Robbins J, Marsh SJ, Brown DA (1993) On the mechanism of M-current inhibition by muscarinic M_1 receptors in DNA-transfected rodent neuroblastoma × glioma cells. J Physiol (Lond) 469:153–178.

Rogalski SL, Chavkin C (2001) Eicosanoids inhibit the G-protein-gated inwardly rectifying potassium channel (Kir3) at the Na^+/PIP_2 gating site. J Biol Chem 276:14855–14860.

Safa P, Boulter J, Hales TG (2001) Functional properties of $Ca_v1.3$ (α_{1D}) L-type Ca^{2+} channel splice variants expressed by rat brain and neuroendocrine GH_3 cells. J Biol Chem 276:38727–38737.

Sanderson MJ, Parker I (2003) Video-rate confocal microscopy. Methods Enzymol 360:447–481.

Shapiro MS, Loose MD, Hamilton SE, Nathanson NM, Gomeza J, Wess J, Hille B (1999) Assignment of muscarinic receptor subtypes mediating G-protein modulation of Ca^{2+} channels by using knockout mice. Proc Natl Acad Sci USA 96:10899–10904.

Shapiro MS, Gomeza J, Hamilton SE, Hille B, Loose MD, Nathanson NM, Roche JP, Wess J (2001) Identification of subtypes of muscarinic receptors that regulate Ca^{2+} and K^+ channel activity in sympathetic neurons. Life Sci 68:2481–2487.

Spector AA (1975) Fatty acid binding to plasma albumin. J Lipid Res 16:165–179.

Suh BC, Hille B (2002) Recovery from muscarinic modulation of M current channels requires phosphatidylinositol 4,5-bisphosphate synthesis. Neuron 35:507–520.

Suh BC, Hille B (2005) Regulation of ion channels by phosphatidylinositol 4,5-bisphosphate. Curr Opin Neurobiol 15:370–378.

Talavera K, Staes M, Janssens A, Droogmans G, Nilius B (2004) Mechanism of arachidonic acid modulation of the T-type Ca^{2+} channel α_{1G}. J Gen Physiol 124:225–238.

Villarroel A (1994) On the role of arachidonic acid in M-current modulation by muscarine in bullfrog sympathetic neurons. J Neurosci 14:7053–7066.

West AE, Griffith EC, Greenberg ME (2002) Regulation of transcription factors by neuronal activity. Nat Rev Neurosci 3:921–931.

Wu L, Bauer CS, Zhen XG, Xie C, Yang J (2002) Dual regulation of voltage-gated calcium channels by $PtdIns(4,5)P_2$. Nature 419:947–952.

Yu SP (1995) Roles of arachidonic acid, lipoxygenases and phosphatases in calcium-dependent modulation of M-current in bullfrog sympathetic neurons. J Physiol (Lond) 487:797–811.

Zhang H, Craciun LC, Mirshahi T, Rohacs T, Lopes CM, Jin T, Logothetis DE (2003) PIP_2 activates KCNQ channels, and its hydrolysis underlies receptor-mediated inhibition of M currents. Neuron 37:963–975.

Zhang Y, Cribbs LL, Satin J (2000) Arachidonic acid modulation of α1H, a cloned human T-type calcium channel. Am J Physiol Heart Circ Physiol 278:H184–H193.